

## Probing Momentum-Dependent Scattering in Uniaxially Stressed $\text{Sr}_2\text{RuO}_4$ through the Hall Effect

Po-Ya Yang<sup>1</sup>, Hilary M. L. Noad<sup>1</sup>, Mark E. Barber,<sup>1,2,3</sup> Naoki Kikugawa,<sup>4</sup> Dmitry A. Sokolov,<sup>1</sup> Andrew P. Mackenzie,<sup>1,5</sup> and Clifford W. Hicks<sup>6,1</sup>

<sup>1</sup>Max Planck Institute for Chemical Physics of Solids, Nöthnitzer Str 40, 01187 Dresden, Germany

<sup>2</sup>Department of Applied Physics, Stanford University, Stanford, California 94305, USA

<sup>3</sup>Geballe Laboratory for Advanced Materials, Stanford, California 94305, USA

<sup>4</sup>National Institute for Materials Science, Tsukuba, Ibaraki 305-0003, Japan

<sup>5</sup>Scottish Universities Physics Alliance, School of Physics and Astronomy, University of St. Andrews, St. Andrews KY16 9SS, United Kingdom

<sup>6</sup>School of Physics and Astronomy, University of Birmingham, Birmingham B15 2TT, United Kingdom



(Received 12 September 2022; accepted 22 June 2023; published 17 July 2023)

The largest Fermi surface sheet of the correlated metal  $\text{Sr}_2\text{RuO}_4$  can be driven through a Lifshitz transition between an electronlike and an open geometry by uniaxial stress applied along the [100] lattice direction. Here, we investigate the effect of this transition on the longitudinal resistivity  $\rho_{xx}$  and the Hall coefficient  $R_H$ .  $\rho_{xx}(T)$ , when  $\text{Sr}_2\text{RuO}_4$  is tuned to this transition, is found to have a  $T^2 \log T$  form, as expected for a Fermi liquid tuned to a Lifshitz transition.  $R_H$  is found to become more negative as the Fermi surface transitions from an electronlike to an open geometry, opposite to general expectations from this change in topology. The magnitude of the change in  $R_H$  implies that scattering changes throughout the Brillouin zone, not just at the point in  $k$  space where the transition occurs. In a model of orbital-dependent scattering, the electron-electron scattering rate on sections of Fermi surface with  $xy$  orbital weight is found to decrease dramatically.

DOI: [10.1103/PhysRevLett.131.036301](https://doi.org/10.1103/PhysRevLett.131.036301)

**Introduction.**—The Hall conductivity of multiband metals is a challenging quantity to analyze. In the low-field limit, it is determined by an integral of the mean free path around the Fermi surfaces [1]. It can therefore be used to probe the momentum dependence of scattering in metals with simple Fermi surfaces [2–4], but as complexity increases models become badly underconstrained. The case of the correlated metal and superconductor  $\text{Sr}_2\text{RuO}_4$  [5] highlights the challenge. With 1% substitution of La onto the Sr site, the low-temperature Hall coefficient changes from electronlike to holelike, even though the Fermi surfaces hardly change [6,7].

The advent of strain tuning might make  $R_H$  a more broadly useful measurement quantity. By correlating changes in  $R_H$  with specific strain-driven changes in electronic structure, models of scattering can be tested with greater rigor. Crucially, if the deformation is elastic the defect landscape is not altered.

Here, we study  $\text{Sr}_2\text{RuO}_4$ , which has become an important test case for the understanding of correlated electron materials [8–10]. It is a highly two-dimensional metal in which correlations renormalize but do not destroy Landau quasiparticles [11,12]. In two dimensions and with field perpendicular to the conducting planes, the Fermi surface integral to determine the Hall conductivity becomes straightforward. Concave sections of Fermi surface contribute positively to the Hall conductivity, and convex sections negatively [1]. The Fermi surfaces of unstressed  $\text{Sr}_2\text{RuO}_4$  are shown in Fig. 1(a). The  $\alpha$  sheet is holelike, while the  $\beta$  and  $\gamma$  sheets are electronlike. Under uniaxial stress  $\sigma$  applied along the [100] lattice direction, the  $\gamma$  sheet transitions to an open geometry, at  $\sigma = \sigma_L \approx -0.75$  GPa, where negative values denote compression. This transition is illustrated in Fig. 1(b). It introduces a necked portion of the  $\gamma$  sheet, where the Fermi surface is concave, and so this transition is in general expected to make the Hall conductivity more positive. If the scattering time is isotropic then the quantitative change might be small, because the Fermi velocity in this necked region is low, but it should still be positive [13,14].

We report here that in fact the change is opposite: the Hall conductivity becomes more negative as the  $\gamma$  sheet topology changes from electronlike to open. The magnitude of the change is large, implying that scattering changes

Published by the American Physical Society under the terms of the Creative Commons Attribution 4.0 International license. Further distribution of this work must maintain attribution to the author(s) and the published article's title, journal citation, and DOI. Open access publication funded by the Max Planck Society.

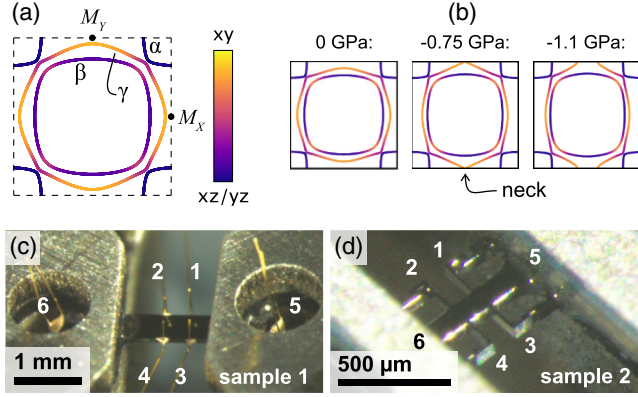


FIG. 1. (a) Model Fermi surfaces of  $\text{Sr}_2\text{RuO}_4$ , colored by orbital weight, from Ref. [15]. (b) Fermi surfaces calculated with a simple tight-binding model, presented later in this Letter, under uniaxial stresses along [100] of 0,  $-0.75$ , and  $-1.1$  GPa. (c),(d) Photographs of samples 1 and 2.

throughout the Brillouin zone.  $\text{Sr}_2\text{RuO}_4$  appears to become a considerably less-strongly correlated metal upon going through this Lifshitz transition, providing a potentially important example of how correlations emerge in metals.

**Methods.**—Measurements were performed using a piezoelectric-driven uniaxial stress device, similar to that described in Ref. [16], that incorporates sensors of both the applied displacement and applied force. As in Ref. [17], a two-part sample carrier allows *in situ* calibration of the zero-force point. Two samples, photographed in Figs. 1(c) and 1(d), were studied. Sample 1 is a beam of constant cross section with electrical contacts attached by hand, while for sample 2 a xenon plasma focused ion beam was used to mill contacts from the sample itself. The residual resistivities are  $0.4$  and  $0.09$   $\mu\Omega\text{-cm}$ , respectively. Because of its lower residual resistivity, most of the data presented here are from sample 2, though some data from sample 1 are included to demonstrate reproducibility.

The Hall effect was measured for field applied along the [001] direction. For both samples, the Hall voltage  $V_H$  at field  $B$  is taken as  $\frac{1}{2}[V_{13}(B) - V_{13}(-B)]$  or  $\frac{1}{2}[V_{24}(B) - V_{24}(-B)]$ , where  $V_{ij} \equiv V_i - V_j$ ,  $V_i$  is the voltage in contact  $i$ , and contact numbering is shown in Figs. 1(c) and 1(d). This procedure cancels contributions to  $V_H$  from contact misalignment. The Hall coefficient is then given by  $R_H = V_H t / (IB)$ , where  $I$  is the applied current and  $t$  the sample thickness.

**Longitudinal resistivity.**—We look first at  $\rho_{xx}(T)$  of  $\text{Sr}_2\text{RuO}_4$  tuned to the Lifshitz transition. The superconductivity of  $\text{Sr}_2\text{RuO}_4$  is strongly enhanced at the Lifshitz transition [18], and so to measure  $\rho_{xx}$  at low temperatures we suppress it with a  $1.5$  T field. We then apply a magnetoresistance model to estimate  $\Delta\rho_{xx}(T)$ , the change in  $\rho_{xx}(T)$  under this  $1.5$  T field. Subtracting  $\Delta\rho_{xx}(T)$  from the data yields an estimate for the longitudinal resistivity

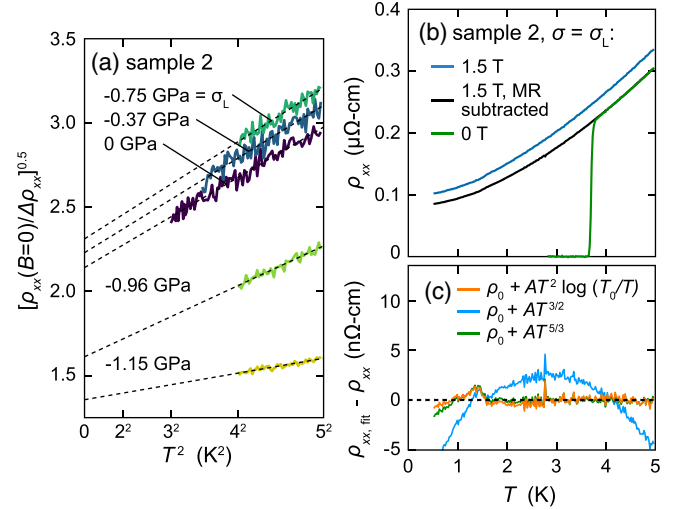


FIG. 2. (a)  $[\rho_{xx}(B=0)/\Delta\rho_{xx}]^{0.5}$ , where  $\Delta\rho_{xx}$  is the change in  $\rho_{xx}$  between 0 and  $1.5$  T, against  $T^2$  for sample 2 at various stresses. The dashed lines are linear fits. (b)  $\rho_{xx}(T)$  of sample 2 at  $\sigma = \sigma_L = -0.75$  GPa and  $B = 0$  and  $1.5$  T. The black line is an estimate of the  $\rho_{xx}(T)$  that would be obtained at  $B = 0$  without superconductivity; it is an average of  $\rho_{xx}$  at  $+1.5$  T with the magnetoresistivity subtracted as described in the text. (c) The difference between various fitting models and the black line in panel (b). For the  $T^2 \log T$  form, the fit yields  $T_0 = 95$  K.

that would be obtained at zero field, if superconductivity did not occur.

For metals with cylindrical, circular Fermi surfaces in weak magnetic fields,

$$\left( \frac{\rho_{xx}(B=0, T)}{\Delta\rho_{xx}(B, T)} \right)^{\frac{1}{2}} \propto (\omega_c \tau)^{-1}, \quad (1)$$

where  $\omega_c$  is the cyclotron frequency  $\omega_c = eB/m^*$  and  $\tau$  is the relaxation time [19]. In general,  $\tau^{-1} \propto \alpha + \beta T^2$  is expected for Fermi liquids. In unstressed  $\text{Sr}_2\text{RuO}_4$  it has been found that  $(\rho_{xx}/\Delta\rho_{xx})^{1/2}$  can be fitted by  $\alpha + \beta T^2$  up to at least  $80$  K [19], even though  $\rho_{xx}$  follows a  $T^2$  form only up to  $\sim 30$  K [19,20]. In Fig. 2(a) we show that this model fits the observed magnetoresistance at each stress that we tested.

We use this model to extrapolate  $\Delta\rho_{xx}(T)$  into the superconducting regime, where it cannot be directly measured. Figure 2(b) shows the measured  $\rho_{xx}(B = 1.5\text{T}, T)$  and  $\rho_{xx}(B = 0, T)$ , at  $\sigma = \sigma_L$ . The black line is  $\rho_{xx}(B = 1.5\text{T}, T) - \Delta\rho_{xx}(T)$ , our estimate for the zero-field resistivity without superconductivity.

We test this zero-field resistivity against three hypotheses. (i)  $\rho_{xx} = \rho_0 + AT^2 \log(T_0/T)$ . This is the form derived from Boltzmann transport theory for a Fermi liquid tuned to a Lifshitz transition. To obtain this form, it is necessary to take into account the fact that only umklapp scattering generates resistivity [21–23]. It is worth noting that for electron-to-open Lifshitz transitions, as we are

considering here, other bands must also be present to yield this form [23]. (ii)  $\rho_{xx} = \rho_0 + AT^{3/2}$ . The non-umklapp scattering rate, which affects, e.g., the thermal but not the electrical resistivity, is expected to scale as  $T^{3/2}$  [23]. (iii)  $\rho_{xx} = \rho_0 + AT^{5/3}$ . This form has been observed near ferromagnetic quantum critical points [24–26]. It is understood theoretically as a result of loss of quasiparticle coherence due to the quantum criticality [25–27].

Figure 2(c) shows the residuals between the data and these fits. The  $T^2 \log T$  and  $T^{5/3}$  forms are seen to work equally well, while the  $T^{3/2}$  form is less good. In contrast, in earlier work the  $T^2 \log T$  and  $T^{3/2}$  forms were found to work equally well, over a fitting range of 4–40 K [28]. We hypothesize that this temperature range was too high to accurately capture the low-temperature behavior. In Ref. [29], we show that an alternative magnetoresistance model,  $(\rho_{xx}/\Delta\rho_{xx})^{1/2} \propto \alpha + \beta T^{3/2}$ , can also be applied at  $\sigma = \sigma_L$ . It does not alter the conclusion that  $\rho_{xx}(T)$  at  $\sigma = \sigma_L$  is well described by the  $T^{5/3}$  or  $T^2 \log T$  form, but not the  $T^{3/2}$  form.

Although the  $T^{5/3}$  and  $T^2 \log T$  models work equally well, the hypothesis under which  $T^{5/3}$  is obtained theoretically, ferromagnetic quantum criticality, appears not to apply here. NMR data on  $\text{Sr}_2\text{RuO}_4$  show that the Stoner factor of  $\text{Sr}_2\text{RuO}_4$  is enhanced by  $\sim 30\%$  at the Lifshitz transition [30], and that there is no dramatic change in quasiparticle weight [31]. Tuning to the Lifshitz transition strengthens ferromagnetic fluctuations, but apparently not to the point that they become critical.

*Hall effect.*—We now turn to the Hall effect. To investigate appropriate measurement fields, in Fig. 3(a) we show  $V_H$  versus  $B$  for sample 2. For temperatures below  $\sim 10$  K, the low-field regime in which  $V_H \propto B$  extends only up to  $\sim 0.3$  T.

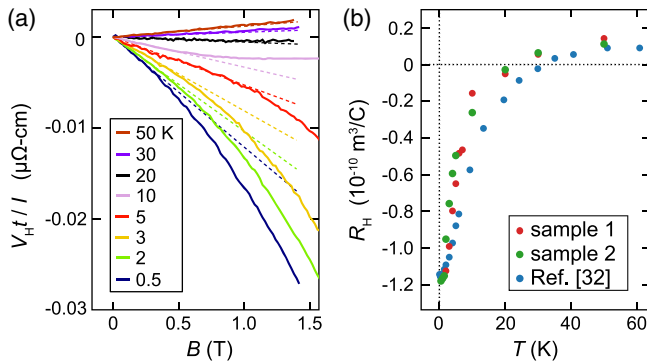


FIG. 3. (a)  $V_H t / I$ , where  $t$  is sample thickness and  $I$  the applied current, versus  $B$  for sample 2 at various temperatures and at zero stress. The dotted lines are extrapolations of linear fits over  $0 < B < 0.35$  T. Equivalent data for sample 1 are shown in Ref. [29]. (b)  $R_H(T)$  of both samples at zero stress, and  $B$  up to  $\pm 0.5$  T for sample 1 and  $\pm 0.35$  T for sample 2. Data from Ref. [32] are also shown.

Figure 3(b) shows  $R_H(T)$  of both samples in the low-field limit. The data are in qualitative agreement with previous reports:  $R_H$  is holelike for temperatures around 50 K, and electronlike below  $\sim 20$  K [32,33].

Figure 4(a) shows  $R_H(\sigma)$  of sample 2 at various temperatures and at  $B = 0.35$  T, which is close to the low-field limit, while Fig. 4(b) shows the equivalent data at 1.5 T, which fully suppresses the superconductivity. Figures 4(c) and 4(d), respectively, show  $\rho_{xx}(\sigma)$  at 0.35 and 1.5 T.

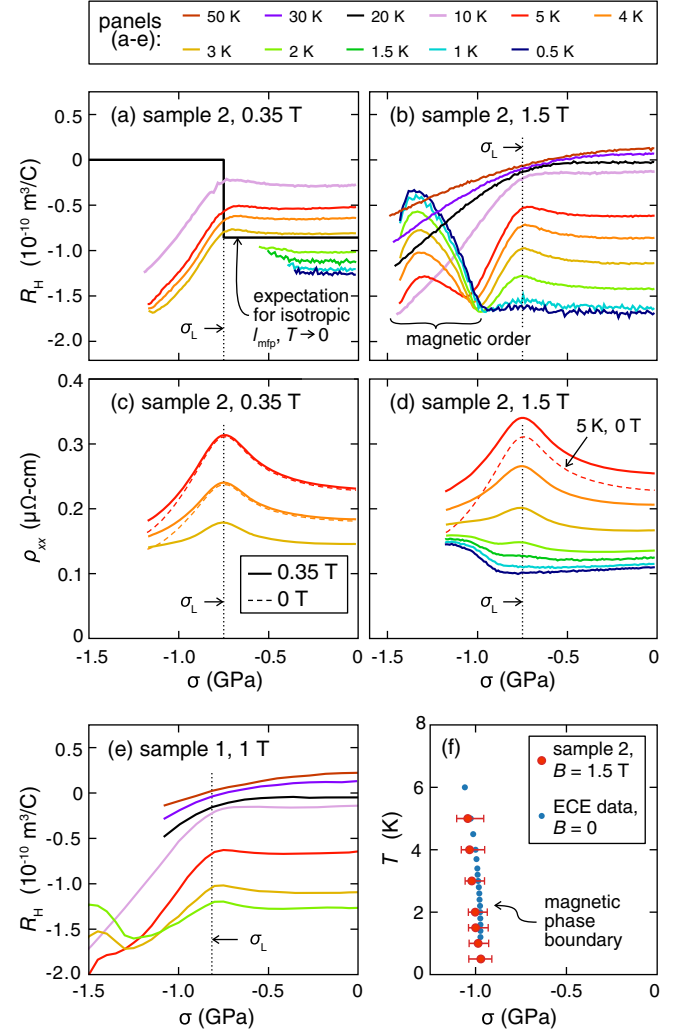


FIG. 4. (a)  $R_H(\sigma)$  of sample 2 at various temperatures, measured at  $B = \pm 0.35$  T. Data that are clearly affected by superconductivity are excluded. The expected  $R_H(\sigma)$  for isotropic mean free path and  $T \rightarrow 0$ , calculated using a simple tight-binding model, is also shown. (b)  $R_H(\sigma)$  of sample 2 at  $B = \pm 1.5$  T, a strong enough field to fully suppress the superconductivity. (c)  $\rho_{xx}(\sigma)$  of sample 2 at  $B = 0$  and 0.35 T. (d)  $\rho_{xx}(\sigma)$  of sample 2 at  $B = 1.5$  T. (e)  $R_H(\sigma)$  of sample 1 at  $B = \pm 1$  T. (f) The phase boundary of the magnetic order, taken as the stresses where  $d^2 R_H / d\sigma^2$  in panel (b) is maximum. The error bars are the FWHM of the peaks in  $d^2 R_H / d\sigma^2$ . Also shown is the phase boundary found in elastocaloric effect (ECE) data [34], with the Lifshitz stress normalized to  $-0.75$  GPa.

Figure 4(e) shows  $R_H(\sigma)$  of sample 1 at 1 T. The stress and temperature dependence of  $R_H$  from sample 1 is similar to that seen from sample 2.

One prominent feature in the 1.5 T  $R_H$  data, in Fig. 4(b), is the stress-induced magnetic order of  $\text{Sr}_2\text{RuO}_4$ , first reported in Ref. [35]. In Fig. 4(f) we show that the phase boundaries found in these 1.5 T  $R_H$  data match well those seen in elastocaloric data at zero field [34]. It is curious, therefore, that  $R_H$  at 0.35 T is not resolvably affected by the magnetic order, even though it is certainly there. This is a point for further investigation.

We identify the Lifshitz stress  $\sigma_L$  by the peak in  $\rho_{xx}$  at 5 K, yielding  $\sigma_L = -0.75 \pm 0.08$  GPa for sample 2. For sample 1,  $\rho_{xx}$  was not measured, but comparison of  $R_H(\sigma)$  with that of sample 2 yields  $\sigma_L = -0.82 \pm 0.08$  GPa. For comparison,  $\sigma_L = -0.71 \pm 0.08$  GPa was reported in Ref. [36].

For temperatures  $\sim 2$  K and above,  $R_H$  from both samples 1 and 2 is seen to become more negative for  $\sigma < \sigma_L$ . As has already been noted, this change is opposite to the expectation based on the change in Fermi surface topology. In Fig. 4(a), we show the expected  $R_H(\sigma)$  assuming an isotropic mean free path, calculated from a tight-binding model that will be presented shortly. With isotropic mean free path,  $R_H$  is a function of Fermi surface topology alone. For  $\sigma < \sigma_L$ , this calculated  $R_H$  is zero because there is one electronlike, one open, and one holelike Fermi surface. The contrast with the data is clear.

Below  $\sim 1$  K, both  $R_H$  and  $\rho_{xx}$  become essentially constant across the Lifshitz transition. The fact that  $R_H(T \rightarrow 0)$  does not change in response to the change in Fermi surface topology indicates that the mean free path must be shorter in the neck region of the  $\gamma$  sheet than elsewhere; even in the  $T \rightarrow 0$  limit, the mean free path does not become isotropic.

*Discussion.*—Our discussion focuses on the Hall effect data at 5 and 10 K, where the downturn in  $R_H$  at  $\sigma < \sigma_L$  is both large and relatively sharp. At these temperatures, the resistivity peaks at  $\sigma \approx \sigma_L$  due to enhanced electron-electron scattering [22,37]. The fact that both the peak in  $\rho_{xx}$  and the downturn  $R_H$  fade away as temperature is reduced below  $\sim 5$  K indicates that it is probably changes in electron-electron scattering that drive the stress dependence of  $R_H$ , too.

To calculate  $R_H$ , followings Refs. [38–40] we employ the simplest possible tight-binding model that reproduces the Fermi surface topology of  $\text{Sr}_2\text{RuO}_4$ . Near-neighbor hopping integrals are taken to vary linearly with strain, with a scaling constant set so that the Lifshitz transition occurs at  $\sigma = -0.75$  GPa. The model Fermi surfaces resulting from this model are those shown in Fig. 1(b). More details are given in Ref. [29]. The Hall conductivity  $\sigma_{xy}$  is calculated using the Ong construction [1]:

$$\sigma_{xy} = \frac{e^3}{2\pi^2\hbar^2} \mathbf{B} \cdot \int_{FS} \frac{d\mathbf{l}_{\text{mfp}}(\mathbf{k}) \times \mathbf{l}_{\text{mfp}}(\mathbf{k})}{2}, \quad (2)$$

where  $\mathbf{l}_{\text{mfp}}(\mathbf{k})$  is the mean free path at point  $\mathbf{k}$ . In words, Eq. (2) states that the Hall conductivity is an integral of the curvature of the Fermi surfaces weighted by  $l_{\text{mfp}} \equiv |\mathbf{l}_{\text{mfp}}|$ . The Hall coefficient  $R_H$  is given by  $R_H \approx (1/B)\sigma_{xy}/(\sigma_{xx}\sigma_{yy})$ .  $\sigma_{xx}$  is taken to be

$$\sigma_{xx} = \frac{e^2}{2\pi^2\hbar} \int_{FS} ds l_{\text{mfp}}(\mathbf{k}) (\hat{\mathbf{l}}_{\text{mfp}}(\mathbf{k}) \cdot \hat{\mathbf{x}})^2, \quad (3)$$

and similarly for  $\sigma_{yy}$ . This equation neglects the distinction between umklapp and non-umklapp processes; it is an approximate model.

In a first, simple test, we set  $l_{\text{mfp}}$  to be isotropic on the two electronlike Fermi sheets,  $\beta$  and  $\gamma$ , but zero on the holelike sheet,  $\alpha$ . This model yields  $R_H = -1.74 \times 10^{-10}$  m<sup>3</sup>/C for unstressed  $\text{Sr}_2\text{RuO}_4$ . The fact that  $R_H$  falls to values in this range when  $\sigma < \sigma_L$  means that  $l_{\text{mfp}}$  must become long on essentially all convex portions of the  $\beta$  and  $\gamma$  sheets relative to  $l_{\text{mfp}}$  on the  $\alpha$  sheets. In other words, scattering must change throughout the Brillouin zone.

We discuss now a more specific model: orbital differentiation. Following Ref. [15], we take the electron-electron scattering rate  $\eta$  to be an orbital-dependent quantity:

$$\eta_\nu(\mathbf{k}) = \sum_m |\langle \chi_m(\mathbf{k}) | \psi_\nu(\mathbf{k}) \rangle|^2 \eta_m. \quad (4)$$

$\nu = \alpha, \beta$ , or  $\gamma$ , while  $m = xz, yz$ , or  $xy$ .  $\eta_\nu$  is the electron-electron scattering rate on Fermi surface  $\nu$ , while  $\eta_m$  is that associated with orbital  $m$ . The key feature of this model is an assumption of local scattering, so that  $\eta_m$  is  $\mathbf{k}$  independent.  $|\langle \chi_m(\mathbf{k}) | \psi_\nu(\mathbf{k}) \rangle|^2$  is the weight of orbital  $m$  in band  $\nu$  at momentum  $\mathbf{k}$ , and the  $\mathbf{k}$  dependence of  $\eta_\nu$  arises solely from the  $\mathbf{k}$  dependence of the orbital weights. This model is supported by photoemission and Raman scattering data [41,42], and applies when Hund's interactions control electronic correlations, as appears to be the case in  $\text{Sr}_2\text{RuO}_4$  [9,10].

For simplicity, we assume  $\eta_{xz} = \eta_{yz} = \eta_{xz,yz}$ , even at nonzero stress where this equality is not symmetry protected.  $R_H$  calculated as a function of the ratio  $\eta_{xy}/\eta_{xz,yz}$  and at three different stresses is shown in Fig. 5(a). Our results at  $\sigma = 0$  match well the more accurate electronic structure model of Ref. [15].  $R_H > 0$  for large  $\eta_{xy}/\eta_{xz,yz}$  because both the  $\beta$  and  $\gamma$  sheets have substantial  $xy$  orbital weight, so a large  $\eta_{xy}$  suppresses the contribution from these sheets, leaving that from the holelike  $\alpha$  sheet.

We use the results shown in Fig. 5(a) to convert  $R_H$  measured at 0.35 T and at 5 and 10 K, temperatures where electron-electron scattering dominates [43], to  $\eta_{xy}/\eta_{xz,yz}$ . Results are shown in Fig. 5(b). At  $\sigma = 0$ , we find  $\eta_{xy}/\eta_{xz,yz} > 1$ . This is in agreement with photoemission data showing that the  $xy$  band is the most strongly renormalized [41]. The electron-electron scattering rate

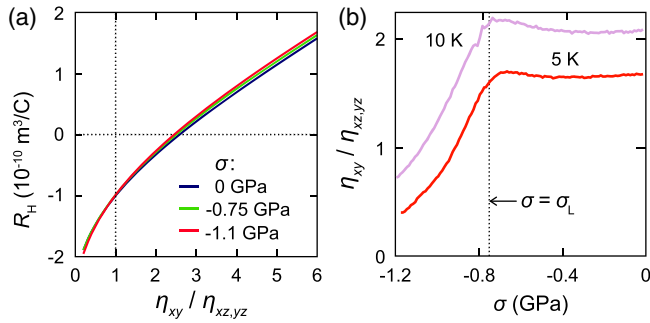


FIG. 5. (a)  $R_H$  calculated within the orbital-dependent scattering model described in the text, as a function of the ratio of  $xy$  and  $xz, yz$  scattering rates,  $\eta_{xy}/\eta_{xz,yz}$ . The calculation employs a simple tight-binding model of the Fermi surfaces of  $\text{Sr}_2\text{RuO}_4$ . (b)  $\eta_{xy}/\eta_{xz,yz}$  versus stress at 5 and 10 K, determined from  $R_H$  of sample 2 at  $\pm 0.35$  T and the calculation results shown in panel (a).

is correlated with the degree of renormalization [44]. Dynamical mean-field theory calculations indicate that this stronger renormalization is due to proximity to the Lifshitz transition [8,9], which occurs in the  $xy$  band.  $\eta_{xy}/\eta_{xz,yz}$  then falls to well below 1 for  $\sigma < \sigma_L$ . Consistent with this interpretation that scattering in the  $xy$  band falls steeply, the magnetoresistivity becomes much stronger for  $\sigma < \sigma_L$ : as seen in Fig. 4(c), at 5 K a substantial difference between  $\rho_{xx}$  at 0 and 0.35 T opens up for  $\sigma < \sigma_L$ . Our data suggest that as  $\text{Sr}_2\text{RuO}_4$  is driven through the Lifshitz transition the  $xy$  band transitions from being the most- to being the least-strongly correlated, and over a remarkably small strain range.

Independent of this specific model, both the large change in  $R_H$  and the increase in magnetoresistivity point to a large change in electron-electron scattering, throughout the Brillouin zone, for  $\sigma < \sigma_L$ . This observation provides potentially important information on the origin of electronic correlations in metals.

Raw data for this publication are available [45].

P. Y. thanks K. Shirer and M. König for assistance with the plasma focused ion beam. We thank A. Georges, M. Zingl, and J. Mravlje for a critical read of the manuscript. We additionally thank E. Berg, N. Hussey, and J. Schmalian for useful comments. We acknowledge the financial support of the Max Planck Society. A. P. M. and C. W. H. acknowledge the financial support of the Deutsche Forschungsgemeinschaft (DFG, German Research Foundation)—TRR 288—422213477 (project A10). N. K. is supported by a KAKENHI Grants-in-Aids for Scientific Research (Grants No. 17H06136, No. 18K04715, and No. 21H01033), and Core-to-Core Program (No. JPJSCCA20170002) from the Japan Society for the Promotion of Science (JSPS) and by a JST-Mirai Program (Grant No. JPMJMI18A3). H. M. L. N. acknowledges support from the Alexander von Humboldt

Foundation through a Research Fellowship for Postdoctoral Researchers. Research in Dresden benefits from the environment provided by the DFG Cluster of Excellence ct.qmat (EXC 2147, project ID 390858940).

- [1] N. P. Ong, *Phys. Rev. B* **43**, 193 (1991).
- [2] N. Nandi, T. Scaffidi, P. Kushwaha, S. Khim, M. E. Barber, V. Sunko, F. Mazzola, P. D. C. King, H. Rosner, P. J. W. Moll, M. König, J. E. Moore, S. Hartnoll, and A. P. Mackenzie, *npj Quantum Mater.* **3**, 66 (2018).
- [3] A. Narduzzo, G. Albert, M. M. J. French, N. Mangkorntong, M. Nohara, H. Takagi, and N. E. Hussey, *Phys. Rev. B* **77**, 220502(R) (2008).
- [4] M. M. J. French, J. G. Analytis, A. Carrington, L. Balicas, and N. E. Hussey, *New J. Phys.* **11**, 055057 (2009).
- [5] Y. Maeno, H. Hashimoto, K. Yoshida, S. Nishizaki, T. Fujita, J. G. Bednorz, and F. Lichtenberg, *Nature (London)* **372**, 532 (1994).
- [6] N. Kikugawa, A. P. Mackenzie, C. Bergemann, R. A. Borzi, S. A. Grigera, and Y. Maeno, *Phys. Rev. B* **70**, 060508(R) (2004).
- [7] N. Kikugawa, A. P. Mackenzie, C. Bergemann, and Y. Maeno, *Phys. Rev. B* **70**, 174501 (2004).
- [8] F. B. Kugler, M. Zingl, H. U. R. Strand, S.-S. B. Lee, J. von Delft, and A. Georges, *Phys. Rev. Lett.* **124**, 016401 (2020).
- [9] J. Mravlje, M. Aichhorn, T. Miyake, K. Haule, G. Kotliar, and A. Georges, *Phys. Rev. Lett.* **106**, 096401 (2011).
- [10] X. Deng, K. M. Stadler, K. Haule, A. Weichselbaum, J. von Delft, and G. Kotliar, *Nat. Commun.* **10**, 2721 (2019).
- [11] C. Bergemann, S. R. Julian, A. P. Mackenzie, S. Nishizaki, and Y. Maeno, *Phys. Rev. Lett.* **84**, 2662 (2000).
- [12] C. Bergemann, A. P. Mackenzie, S. R. Julian, D. Forsythe, and E. Ohmichi, *Adv. Phys.* **52**, 639 (2003).
- [13] A. V. Maharaj, I. Esterlis, Y. Zhang, B. J. Ramshaw, and S. A. Kivelson, *Phys. Rev. B* **96**, 045132 (2017).
- [14] E. K. Kokkinis, G. Goldstein, D. V. Efremov, and J. J. Betouras, *Phys. Rev. B* **105**, 155123 (2022).
- [15] M. Zingl, J. Mravlje, M. Aichhorn, O. Parcollet, and A. Georges, *npj Quantum Mater.* **4**, 35 (2019).
- [16] M. A. Barber, A. Steppke, A. P. Mackenzie, and C. W. Hicks, *Rev. Sci. Instrum.* **90**, 023904 (2019).
- [17] F. Jerzembeck, H. S. Røising, A. Steppke, H. Rosner, D. A. Sokolov, N. Kikugawa, T. Scaffidi, S. H. Simon, A. P. Mackenzie, and C. W. Hicks, *Nat. Commun.* **13**, 4596 (2022).
- [18] A. Steppke, L. Zhaox, M. E. Barber, T. Scaffidi, F. Jerzembeck, H. Rosner, A. S. Gibbs, Y. Maeno, S. H. Simon, A. P. Mackenzie, and C. W. Hicks, *Science* **355**, eaaf9398 (2017).
- [19] N. E. Hussey, A. P. Mackenzie, J. R. Cooper, Y. Maeno, S. Nishizaki, and T. Fujita, *Phys. Rev. B* **57**, 5505 (1998).
- [20] Y. Maeno, K. Yoshida, H. Hashimoto, S. Nishizaki, S.-I. Ikeda, M. Nohara, T. Fujita, A. P. Mackenzie, N. E. Hussey, J. G. Bednorz, and F. Lichtenberg, *J. Phys. Soc. Jpn.* **66**, 1405 (1997).
- [21] R. Hlubina, *Phys. Rev. B* **53**, 11344 (1996).
- [22] C. H. Mousatov, E. Berg, and S. A. Hartnoll, *Proc. Natl. Acad. Sci. U.S.A.* **117**, 2852 (2020).

- [23] V. C. Stangier, E. Berg, and J. Schmalian, *Phys. Rev. B* **105**, 115113 (2022).
- [24] M. Nicklas, M. Brando, G. Knebel, F. Mayr, W. Trinkl, and A. Loidl, *Phys. Rev. Lett.* **82**, 4268 (1999).
- [25] R. P. Smith, M. Sutherland, G. G. Lonzarich, S. S. Saxena, N. Kimura, S. Takashima, M. Nohara, and H. Takagi, *Nature (London)* **455**, 1220 (2008).
- [26] M. Sutherland, R. P. Smith, N. Marcano, Y. Zou, S. E. Rowley, F. M. Grosche, N. Kimura, S. M. Hayden, S. Takashima, M. Nohara, and H. Takagi, *Phys. Rev. B* **85**, 035118 (2012).
- [27] J. Mathon, *Proc. R. Soc. A* **306**, 355 (1968).
- [28] M. E. Barber, A. S. Gibbs, Y. Maeno, A. P. Mackenzie, and C. W. Hicks, *Phys. Rev. Lett.* **120**, 076602 (2018).
- [29] See Supplemental Material at <http://link.aps.org/supplemental/10.1103/PhysRevLett.131.036301> for additional data on sample mounting, further experimental data, and a description of the tight-binding model.
- [30] Y. Luo, A. Pustogow, P. Guzman, A. P. Dioguardi, S. M. Thomas, F. Ronning, N. Kikugawa, D. A. Sokolov, F. Jerzembeck, A. P. Mackenzie, C. W. Hicks, E. D. Bauer, I. I. Mazin, and S. E. Brown, *Phys. Rev. X* **9**, 021044 (2019).
- [31] A. Chronister, M. Zingl, A. Pustogow, Y. Luo, D. A. Sokolov, F. Jerzembeck, N. Kikugawa, C. W. Hicks, J. Mravlje, E. D. Bauer, J. D. Thompson, A. P. Mackenzie, A. Georges, and S. E. Brown, *npj Quantum Mater.* **7**, 113 (2022).
- [32] A. P. Mackenzie, N. E. Hussey, A. J. Diver, S. R. Julian, Y. Maeno, S. Nishizaki, and T. Fujita, *Phys. Rev. B* **54**, 7425 (1996).
- [33] N. Shirakawa, K. Murata, Y. Nishihara, S. Nishizaki, Y. Maeno, T. Fujita, J. G. Bednorz, F. Lichtenberg, and N. Hamada, *J. Phys. Soc. Jpn.* **64**, 1072 (1995).
- [34] Y.-S. Li, M. Garst, J. Schmalian, N. Kikugawa, D. A. Sokolov, C. W. Hicks, F. Jerzembeck, M. S. Ikeda, A. W. Rost, M. Nicklas, and A. P. Mackenzie, *Nature (London)* **607**, 276 (2022).
- [35] V. Grinenko, S. Ghosh, R. Sarkar, J.-C. Orain, A. Nikitin, M. Elender, D. Das, Z. Guguchia, F. Brückner, M. E. Barber, J. Park, N. Kikugawa, D. A. Sokolov, J. S. Bobowski, T. Miyoshi, Y. Maeno, A. P. Mackenzie, H. Luetkens, C. W. Hicks, and H.-H. Klauss, *Nat. Phys.* **17**, 748 (2021).
- [36] M. E. Barber, F. Lechermann, S. V. Streltsov, S. L. Skornyakov, S. Ghosh, B. J. Ramshaw, N. Kikugawa, D. A. Sokolov, A. P. Mackenzie, C. W. Hicks, and I. I. Mazin, *Phys. Rev. B* **100**, 245139 (2019).
- [37] F. Herman, J. Buhmann, M. H. Fischer, and M. Sigrist, *Phys. Rev. B* **99**, 184107 (2019).
- [38] V. B. Zabolotnyy, D. V. Evtushinsky, A. A. Kordyuk, T. K. Kim, E. Carleschi, B. P. Doyle, R. Fittipaldi, M. Cuoco, A. Vecchione, and S. V. Borisenko, *J. Electron Spectrosc. Relat. Phenom.* **191**, 48 (2013).
- [39] A. T. Rømer, D. D. Scherer, I. M. Eremin, P. J. Hirschfeld, and B. M. Andersen, *Phys. Rev. Lett.* **123**, 247001 (2019).
- [40] S. Cobo, F. Ahn, I. Eremin, and A. Akbari, *Phys. Rev. B* **94**, 224507 (2016).
- [41] A. Tamai, M. Zingl, E. Rozbicki, E. Cappelli, S. Riccò, A. de la Torre, S. McKeown Walker, F. Y. Bruno, P. D. C. King, W. Meevasana, M. Shi, M. Radović, N. C. Plumb, A. S. Gibbs, A. P. Mackenzie, C. Berthod, H. U. R. Strand, M. Kim, A. Georges, and F. Baumberger, *Phys. Rev. X* **9**, 021048 (2019).
- [42] J.-C. Philippe, B. Baptiste, C. Sow, Y. Maeno, A. Forget, D. Colson, M. Cazayous, A. Sacuto, and Y. Gallais, *Phys. Rev. B* **103**, 235147 (2021).
- [43] X. Deng, K. Haule, and G. Kotliar, *Phys. Rev. Lett.* **116**, 256401 (2016).
- [44] X. Deng, A. Sternbach, K. Haule, D. N. Basov, and G. Kotliar, *Phys. Rev. Lett.* **113**, 246404 (2014).
- [45] C. W. Hicks, Raw data supporting the article “Probing Momentum-Dependent Scattering in Uniaxially Stressed  $\text{Sr}_2\text{RuO}_4$  through the Hall Effect”, [10.25500/edata.bham.00000973](https://doi.org/10.25500/edata.bham.00000973).